Elisabeth J. Faber
J. Albert van Kuik
Johannis P. Kamerling
Johannes F. G. Vliegenthart
Bijvoet Center,
Department of Bio-Organic Chemistry,
Utrecht University,
PO Box 80.075,
NL-3508 TB Utrecht,
The Netherlands

Received 18 January 2001;
accepted 18 July 2001

Modeling of the Structure in Aqueous Solution of the Exopolysaccharide Produced by *Lactobacillus helveticus* 766

Abstract: *A method is described for constructing a conformational model in water of a heteropolysaccharide built up from repeating units, and is applied to the exopolysaccharide produced by* Lactobacillus helveticus *766. The molecular modeling method is based on energy minima, obtained from molecular mechanics calculations of each of the constituting disaccharide fragments of the repeating unit in vacuo, as starting points. Subsequently, adaptive umbrella sampling of the potential of mean force is applied to extract rotamer populations of glycosidic dihedral angles of oligosaccharide fragments in solution. From these analyses, the most probable conformations are constructed for the hexasaccharide-repeating unit of the polysaccharide. After exploring the conformational space of each of the individual structures by molecular dynamics simulations, the different repeating unit conformations are used as building blocks for the generation of oligo- and polysaccharide models, by using a polysaccharide building program. The created models of the exopolysaccharide produced by* L. helveticus *766 exhibit a flexible twisted secondary structure and tend to adopt a random coil conformation as tertiary structure.* © 2002 John Wiley & Sons, Inc. Biopolymers 63: 66–76, 2002

Keywords: *adaptive umbrella sampling; conformation analysis; exopolysaccharide;* Lactobacillus helveticus*; molecular modeling; potential of mean force*

INTRODUCTION

Polysaccharides are essential elements of life, having a large number of different functions in plants, animals, and microorganisms.[1] Although the physiological function of microbial exopolysaccharides (EPSs) produced by lactic acid bacteria is hardly understood, the interest of the food industry in their texturizing properties in fermented dairy products is increasing.[2] In order to get insight into the relationship between

Correspondence to: J. P. Kamerling; email: kame@boc.chem.uu.nl.

Contract grand sponsor: Ministry of Economic Affairs and the Integral Structure Plan for the Northern Netherlands from the Dutch Development Company

Biopolymers, Vol. 63, 66–76 (2002)

DOI 10.1002/bip.1063

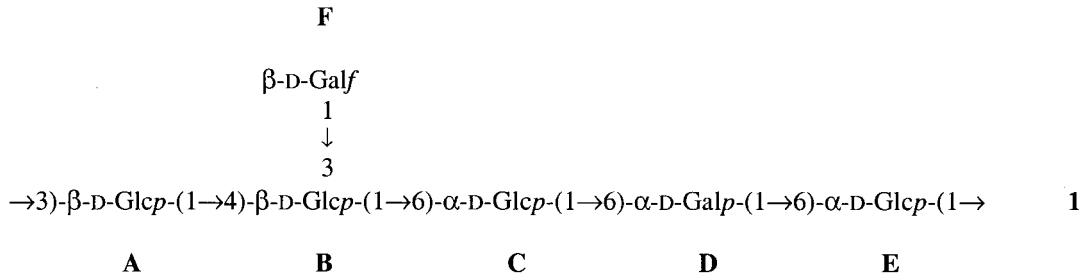

SCHEME 1

the structures of EPSs produced by lactic acid bacteria and their physical properties, in addition to the primary structures,[3] the secondary and tertiary structures of the EPSs have to be elucidated. For helix forming carbohydrate polymers, X-ray diffraction patterns from polycrystalline and oriented fibers and films can be interpreted in terms of reliable three-dimensional models.[4] NMR spectroscopy and computational methods can be used to obtain conformational data of these polymers in solution. A typical example of the modeling of bacterial polysaccharides in vacuo, is the prediction of hollow helical structures for the EPS produced by *Lactobacillus sake* 0-1.[5] In the last study, low energy conformations of the pentasaccharide repeating unit were extrapolated to regular polysaccharide structures using a polysaccharide builder program. In a more complete investigation, a combination of molecular modeling and NMR spectroscopy was used to derive the conformation of the polysaccharide produced by *Streptococcus mitis* J22.[6] The applied NMR techniques involved uniform ^{13}C enrichment of the polysaccharide, which allowed for accurate measurements of heteronuclear $^{3}J_{CH}$ values. These data were used to generate starting conformations for molecular dynamics simulations in vacuo.

Here, we report on the development of a method to calculate the secondary and tertiary structures of polysaccharides consisting of repeating units, by taking into account solvent effects by explicitly including water molecules. The method includes molecular mechanics (MM) calculations, adaptive umbrella sampling (AUS) of the potential of mean force (PMF), and molecular dynamics (MD) simulations. The repetitious nature of the polysaccharides enables to begin with the exploration of the conformational space of small fragment molecules that are gradually elongated. Finally, the obtained results are extrapolated to molecules of the size of 50 and 500 backbone residues. The method is applied to EPS **1**, produced by the lactic acid bacterium *Lactobacillus helveticus* 766, which is a homofermentative thermophilic lactic acid bacterium used in the manufacturing of various cheeses.[7] (See Scheme 1.)

MATERIALS AND METHODS

Nomenclature

For the three staggered conformations of the C_5—C_6 bonds, the notation *tg*, *gt*, and *gg* is used. In this nomenclature *g* and *t* are abbreviations of *gauche* (±60°) and *trans* (180°), respectively, indicating qualitatively the value of a dihedral angle. The angle of the O_6—C_6—C_5—O_5 moiety is indicated by the first character and the angle of the O_6—C_6—C_5—C_4 moiety by the second.

Molecular Mechanics Calculations

Minimal energy calculations in vacuo were performed with CHEAT,[8,9] a CHARMm based force field for carbohydrates. In this force field, hydroxyl groups are represented by extended atoms to prevent intramolecular hydrogen bond formation in vacuo. Minimal energy contour plots were calculated on a 5° by 5° grid and were plotted at intervals of 1 kcal/mol with respect to the calculated global energy minimum.

Adaptive Umbrella Sampling of the PMF

PMF calculations[10] were performed with the GROMOS force field using the method of adaptive umbrella sampling. All simulations were divided into jobs of 10 ps. Dihedral angle values were partitioned into 72 classes, each having a width of 5°. The derivative of the PMF was evaluated as a 12-term Fourier series. Each system was simulated for 10 ns, and the final PMF for each system was used to obtain the rotamer population distributions of the sampled dihedral angle.

Molecular Dynamics

MD simulations in water were performed using the GROMOS program[11] with the improved force field for carbohydrates.[12] Each repeating unit was placed in a computational

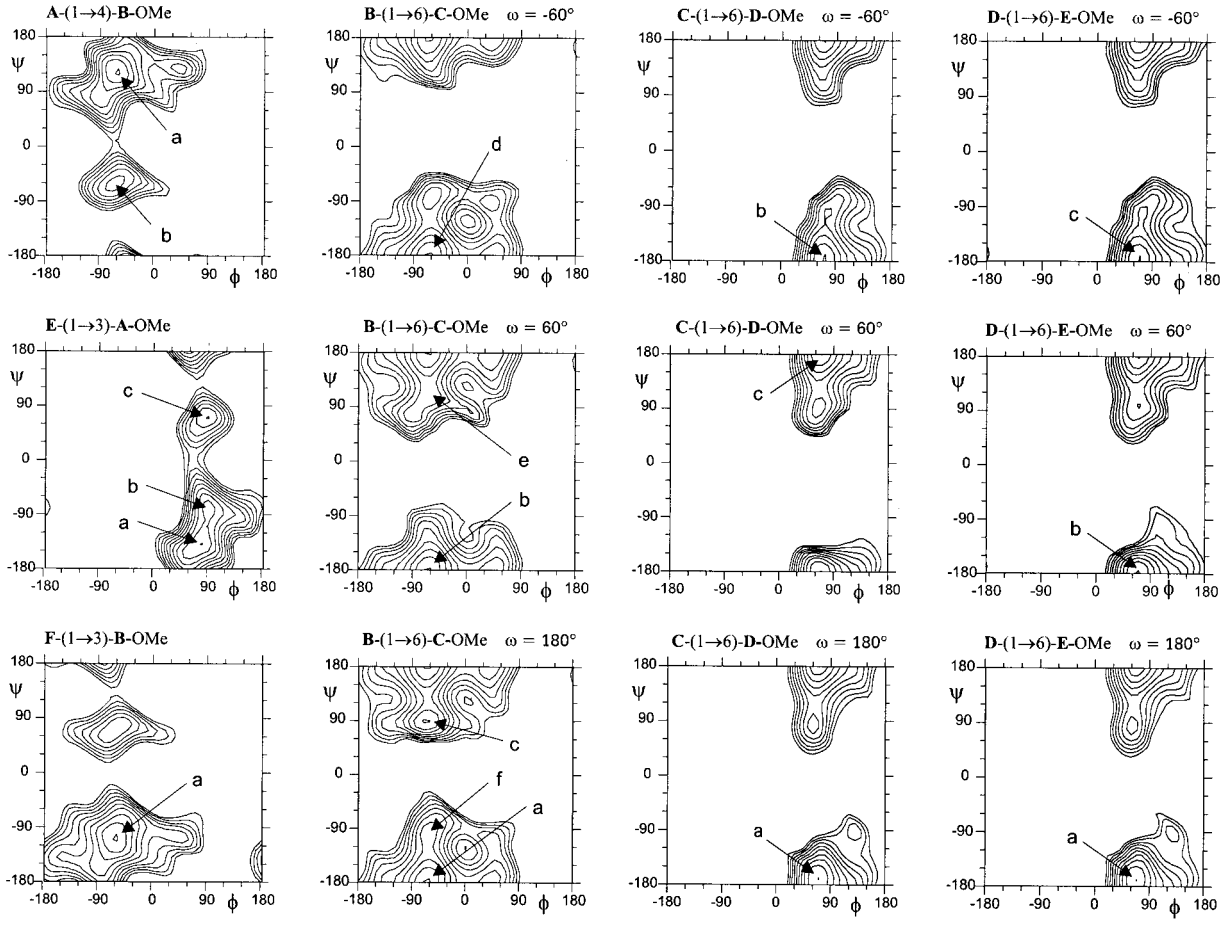

FIGURE 1 Energy contour plots for each of the constituting disaccharides of the *L. helveticus* 766 EPS. Contours are plotted at regular intervals of 1 up to 10 kcal/mol with respect to the global energy minimum. Global minima are indicated with a and local minima that are at the most 3 kcal/mol higher than the global minima are indicated with b–f.

truncated octahedral periodic box containing between 1075 and 1781 SPC/E[13] water molecules. All bond lengths were kept fixed using the SHAKE procedure.[14] Simulations were performed at constant temperature (300 K) and pressure (1 atm) with a relaxation time of 0.1 and 0.5 ps, respectively. For the simulations a cut-off radius of 0.8 nm, a time step of 2 fs and a total simulation time of 1 ns was used. A hydrogen bond is considered to be present for hydrogen and acceptor oxygen atoms with an O—H · · · O distance of less than 2.5 Å and a bond angle larger than 120°.

Polysaccharide Building

From the conformational ensembles I–VIII, obtained by MD simulations, polysaccharide models were generated using an in-house made building program. In brief, the program selects at random elongated repeating units. The selected repeating units are connected from residue **E** of the first repeating unit to residue **A** of the second**,** using the dihedral angles ϕ of $\mathbf{E} \rightarrow \mathbf{A}''$ and ψ of $\mathbf{E}' \rightarrow \mathbf{A}$. The overlapping monosaccharide residues $\mathbf{E}'$, $\mathbf{A}''$, and $\mathbf{B}''$ are removed. After assembling each repeating unit, the polymer is checked for occupied space violations, and if necessary repeating units are rearranged or the polysaccharide is rebuilt.

RESULTS AND DISCUSSION

As a first approach in calculating repeating unit containing polysaccharide conformations, it is assumed that monosaccharide residues separated by at least one repeating unit in the polysaccharide chain are not in close spatial contact and therefore do not influence each others behavior. This strategy allows for the conformational investigation of a repeating unit on both sides elongated by monosaccharides of neighboring repeating units. The results can then be extrap-

Table I Minimal Energy Conformations of the Six Constituting Disaccharide Fragments of *L. helveticus* 766 EPS

Disaccharide Fragments		Minima	Dihedral Angles ϕ	ψ	ω	ΔE[a]
A-(1 → 4)-**B**	β-D-Glc*p*-(1 → 4)-β-D-Glc*p*–OMe	a	−60	119	—	0.0
		b	−55	−53	—	2.7
B-(1 → 6)-**C**	β-D-Glc*p*-(1 → 6)-α-D-Glc*p*–OMe	a	−64	178	−178	0.0
		b	−64	178	61	0.0
		c	−62	91	−178	0.7
		d	−65	179	−68	1.3
		e	−77	84	44	1.3
		f	−61	−90	171	2.1
C-(1 → 6)-**D**	α-D-Glc*p*-(1 → 6)-α-D-Gal*p*–OMe	a	68	−170	−172	0.0
		b	67	−176	−58	1.3
		c	66	180	70	1.7
D-(1 → 6)-**E**	α-D-Gal*p*-(1 → 6)-α-D-Glc*p*–OMe	a	67	−168	−178	0.0
		b	67	−177	61	0.3
		c	67	−176	−68	2.1
E-(1 → 3)-**A**	α-D-Glc*p*-(1 → 3)-β-D-Glc*p*–OMe	a	78	−139	—	0.0
		b	90	−80	—	0.6
		c	87	73	—	2.9
F-(1 → 3)-**B**	β-D-Gal*f*-(1 → 3)-β-D-Glc*p*–OMe	a	−63	−107	—	0.0

[a] Relative energy (kcal/mol).

olated to the conformation of the polysaccharide. After the determination of the abundance of the various conformations of the repeating unit, the flexibilities of these conformations are explored by MD simulations, and from these results, polysaccharide structures are constructed. At this stage, occupied space violations of monosaccharides belonging to different repeating units are taken into account.

Molecular Mechanics Calculations

Due to the relative rigidity of the monosaccharide rings, the conformational differences in the polysaccharide backbone originate mainly from the glycosidic dihedral angles, and therefore these angles are investigated first. Minimal energy calculations of the six constituting disaccharide fragments of the polysaccharide repeating unit are performed in vacuo using the CHEAT force field.[8,9] For each of the disaccharides β-D-Glc*p*-(1 → 4)-β-D-Glc*p*–OMe (**A** → **B**), α-D-Glc*p*-(1 → 3)-β-D-Glc*p*–OMe (**E** → **A**), and β-D-Gal*f*-(1 → 3)-β-D-Glc*p*–OMe (**F** → **B**) the glycosidic dihedral angles ϕ (O_{5M}—C_{1M}—O_{XN}—C_{XN}), and ψ (C_{1M}—O_{XN}—C_{XN}—$C_{(X-1)N}$] must be considered,[15] and potential energy maps are generated to determine the lowest energy conformations for these glycosidic angles. For the (1 → 6)-linked disaccharides β-D-Glc*p*-(1 → 6)-α-D-Glc*p*–OMe (**B** → **C**), α-D-Glc*p*-(1 → 6)-α-D-Gal*p*–OMe (**C** → **D**), and α-D-Gal*p*-(1 → 6)-α-D-Glc*p*–OMe (**D** → **E**), the additional glycosidic dihedral angle ω (O_{6N}—C_{6N}—C_{5N}—C_{4N}) is involved.[15] Here, three separate minimal energy calculations are performed for the ϕ and ψ glycosidic angles, reflecting the *gauche–gauche* (*gg*), *gauche–trans* (*gt*), and *trans–gauche* (*tg*) orientations of the ω angle. The potential energy maps for each of the investigated disaccharides are presented in Figure 1. In each map, the global energy minimum, as well as the different local energy minima are indicated. The glycosidic dihedral angles and energy minima with energies that are at the most 3 kcal/mol higher than the global minima are listed in Table I. Inspection of the energy minima of the different potential energy surfaces of the glycosidic linkages shows that for the disaccharides **A** → **B** and **E** → **A** the main flexibilities can be attributed to the dihedral angles ψ, for the disaccharides **B** → **C** and **C** → **D** to both ψ and ω, and for the disaccharide **D** → **E** to ω. Furthermore, **F** → **B** is the least flexible disaccharide in having only one energy minimum.

Adaptive Umbrella Sampling of the PMF

In order to study the rotamer distribution of the ψ and ω glycosidic angles in water, PMF calculations[10] are

Table II Probability Distribution[a] of the ψ and ω Dihedral Angles of the Six Constituting Disaccharide Fragments of *L. helveticus* 766 EPS

Dihedral Angle	**A**-(1 → 4)-**B**	**B**-(1 → 6)-**C**	**C**-(1 → 6)-**D**	**D**-(1 → 6)-**E**	**E**-(1 → 3)-**A**	**F**-(1 → 3)-**B**
ψ						
	120 (>98)	180 (82)	180 (89)	−170 (>98)	−130 (>98)	−100 (>98)
		80 (16)	80 (10)			
		−75 (2)	−90 (1)			
ω						
(*gt*)	—	−170 (69)	−170 (87)	−170 (70)	—	—
(*gg*)	—	60 (29)	70 (5)	60 (28)	—	—
(*tg*)	—	−80 (2)	−70 (8)	−80 (2)	—	—

[a] Probability distributions are given in parentheses in %.

performed with the GROMOS force field using the method of adaptive umbrella sampling (AUS). The umbrella potential is applied to only one dihedral angle. In order to obtain a correct rotamer distribution of this dihedral angle, the unrestricted dihedral angles need to be sampled sufficiently during the AUS simulations. This is feasible, when the global energy minimum for this dihedral is much lower than the other minima, rendering the latter contributions negligible. Similarly, when low energy barriers between global and local minima make frequent transitions possible during an AUS simulation, it results in the conformational exploration of all minima. Starting structures for the AUS simulations are created with the glycosidic dihedral angles corresponding to the lowest energy conformations. To include possible interactions of monosaccharides that are close in space, most calculations are performed on oligosaccharide fragments larger than disaccharides. However, the total number of monosaccharide residues is limited to four, to keep the simulation period within 10 ns. All Fourier coefficients have converged after this period, which indicates that the total sampling time has been sufficiently long. The optimal sizes of the selected fragments are deduced by iterative processes as follows. In a first approach, disaccharide fragments are used for the AUS simulations. The whole protocol is repeated with a larger fragment if in the modeling procedure interactions to neighboring residues became apparent. Finally, the ψ angle of **E** → **A** is evaluated using the methyl glycoside analog of the disaccharide fragment. The ψ angles of **A** → **B** and **F** → **B** are evaluated separately using the trisaccharide **A** → [**F** →]**B**–OMe, and the ψ and ω angles of **B** → **C**, **C** → **D**, and **D** → **E** using the trisaccharides **B** → **C** → **D**–OMe, and **C** → **D** → **E**–OMe, and the tetrasaccharide **D** → **E** → **A** → **B**–OMe, respectively.

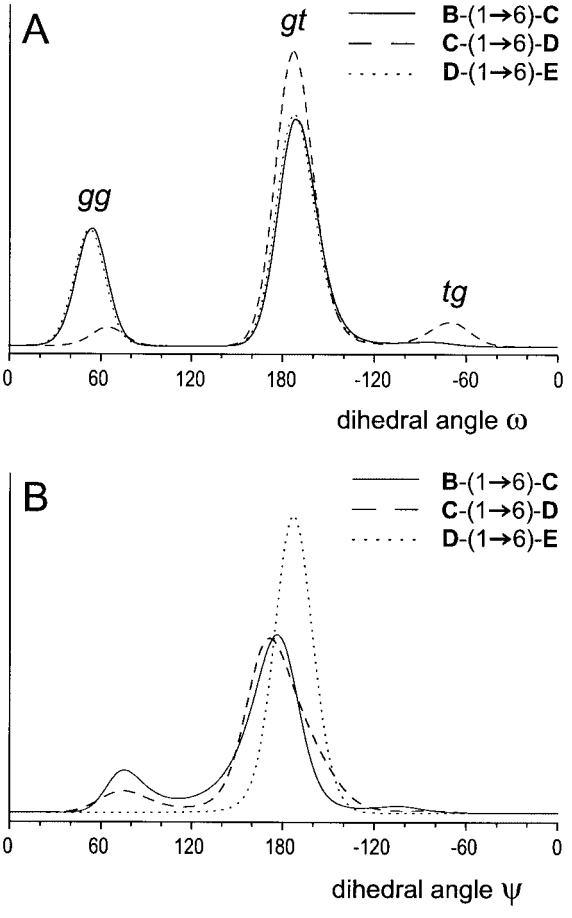

FIGURE 2 Probability distribution profiles of dihedral angles (A) ω and (B) ψ of the (1 → 6)-linked fragments of the *L. helveticus* EPS, obtained by PMF calculations in water.

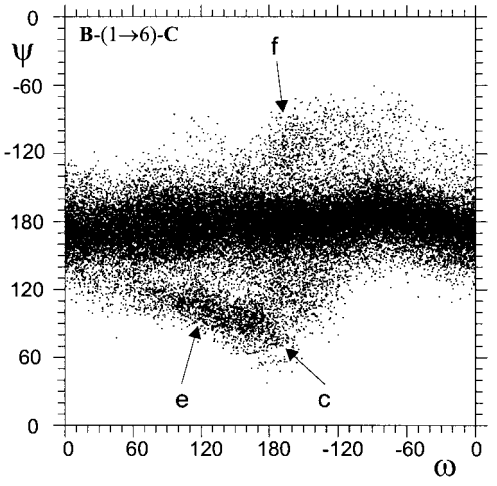

FIGURE 3 Scatter plot of the ψ and ω dihedral angles of the AUS simulation of the ω dihedral angle in the **B** → **C** fragment.

In Table II probability distributions calculated from the free energy differences are presented. For the ϕ dihedral angles, no transitions are observed in any of the AUS simulations. This is consistent with the potential energy maps (Figure 1), which show single minimum-energy regions for the ϕ angles. Therefore, it is assumed that during 10 ns AUS simulations the conformational space of ϕ is adequately explored. For element **A** → **B**, the results are consistent with the conformational analysis data of β-cellobioside.[16] This disaccharide occupies primarily one minimum-energy region ($\phi/\psi = -90°/120°$), whereas only one other stable conformational region exists ($\phi/\psi = -90°/-50°$). This second minimum-energy region does not differ from the primary minimum-energy region with respect to the ϕ dihedral angle, confirming the main flexibility to be located in the ψ angle of element **A** → **B**. From the combined results of these AUS runs it emerges that the **E** → **A** → [**F** →]**B** structural element essentially adopts one conformation with **E** → **A** $\phi/\psi = 100°/-130°$, **A** → **B** $\phi/\psi = -90°/120°$, and **F** → **B** $\phi/\psi = -80°,-100°$. The distribution profiles of the ω angles of the (1 → 6)-linked disaccharide fragments (Figure 2A) show that the → 6)-α-D-Glc*p* fragments of **B** → **C** and **D** → **E** adopt both the *gg* and *gt* conformation. These conformations occur in ratios similar to the rotamer distribution about the C_5—C_6 bond in gentiobiose [β-D-Glc*p*-(1 → 6)-D-Glc*p*]: *gg* (34%), *gt* (66%).[17] In the distribution profile of the → 6)-α -D-Gal*p* fragment of **C** → **D**, ω is located mainly in the *gt* orientation. This is in agreement with the probability distribution of the hydroxy-methyl group of free β-D-Gal*p*: *gt* (70%), *tg* (25%).[12] The resemblance of the calculated and published dihedral angle ratios of the smaller fragments reveals that monosaccharide residues that are not directly involved in the sampled glycosidic linkage have only a small effect on the rotamer distribution. Further analysis of the AUS trajectories reveals rapid transitions as well as distinct dihedral angle populations for the free ψ angles during the AUS of the ω angles. This shows that ψ is adequately sampled and that correlations exist between the ψ and ω dihedral angles. As an example of these observations, a scatter plot of the sampled ω angle vs the corresponding free ψ angle of the **B** → **C** fragment is presented in Figure 3. The local minima c, e, and f, obtained from the minimal energy calculations are all represented. The distribution profiles of the ψ angles of the (1 → 6)-linked disaccharide fragments (Figure 2B) show that ψ is predominantly 180° and the **B** → **C** and **C** → **D** fragments reveal an additional population of ψ around 60°. A relatively low energy barrier between both populations suggests flexibility in the ψ angle. In

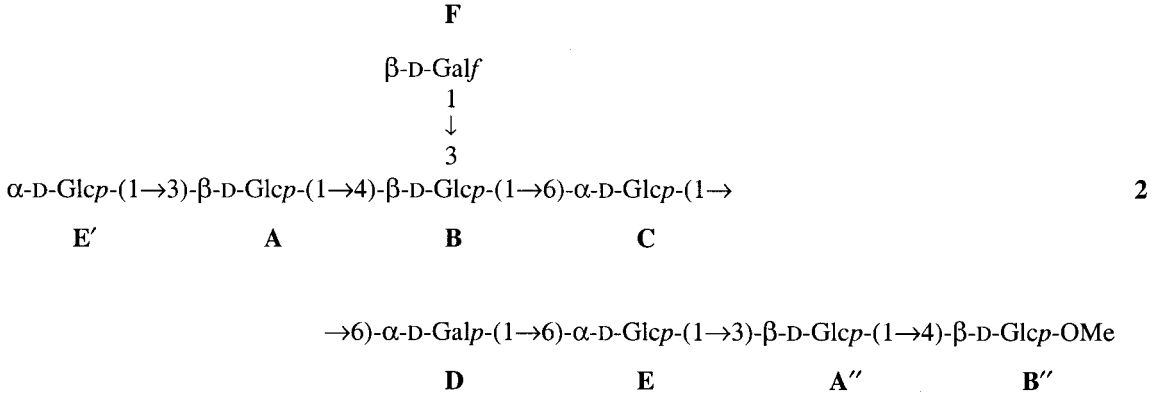

SCHEME 2.

Table III Orientation of the ω Dihedral Angles and Probability of the Local Minimum-Energy Conformations I–VIII for Structure 2

Fragment	I	II	III	IV	V	VI	VII	VIII
				Orientation				
B-(1 → 6)-**C**	−170	60	−170	60	−170	−170	60	−170
C-(1 → 6)-**D**	−170	−170	−170	−170	−70	70	−70	−70
D-(1 → 6)-**E**	−170	−170	60	60	−170	−170	−170	60
				Probability (%)				
	45	19	18	7	4	3	2	2

contrast, the distribution profiles of the ω angles indicate high energy barriers between *gg*, *gt*, and *tg* (Figure 2A). During the AUS of the ψ angles, the trajectories of the free ω angles show between one and three transitions only, confirming that the high energy barriers between the ω populations make adequate sampling of these free angles difficult. Therefore, it is assumed that the AUS simulations of ψ from the (1 → 6)-linkages are less reliable than those of ω.

The conformational preferences, resulting from the PMF calculations, are used to create starting structures for the MD simulations.[11–14] For the (1 → 6)-linkages, only the distribution information of ω angles is used. This is permitted, since the flexibility of the ψ angles is expected to allow adequate sampling in the free MD simulations. In order to include all glycosidic linkages present in the EPS, and to consider possible influences of monosaccharides from adjacent repeating units, the repeating unit of the EPS is elongated with two residues at the reducing side and with one at the nonreducing side (**2**). It should be noted that elongated repeating unit **2** is chosen in such a way that the most flexible part is in the center. (See Scheme 2.)

Based on the rotamer distributions obtained from the AUS runs of the ω angles (Table II), the eight most probable conformations (I–VIII) are constructed (Table III). The ϕ and ψ angles are started in their global energy minima (Table I) and their conformational behavior is taken into account in the MD simulations. In Figure 4 the differences are illustrated between the eight constructed conformations. The structures include a ribbon, which is drawn through the glycosidic bonds, perpendicular on the C_{1M}—O_{XN}—C_{XN} plane, to visualize the backbone of the molecule. All conformers show some bends or twists; for example, V and VIII have a back-folded conformation in which several residues come into close contact.

Molecular Dynamics Simulations

In order to sample the conformational space of I–VIII, MD simulations in water[11–14] of 1 ns are performed and the trajectory-averaged dihedral angles are listed in Table IV. Inspection of the MD trajectories reveals flexibility within the conformations as illustrated by

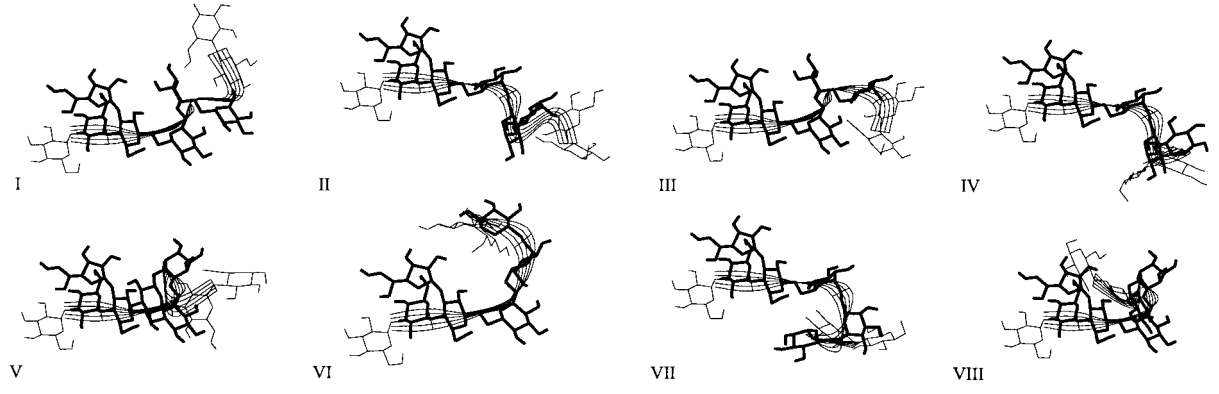

FIGURE 4 Local minimum-energy conformations of the eight most probable conformational families (I–VIII) found by PMF calculations of **2**. Ribbons are drawn through the glycosidic bonds, perpendicular on the C_{1M}—O_{XN}—C_{XN} plane, to visualize the backbone of the molecule.

Table IV Trajectory-Averaged Dihedral Angles of the MD Simulations for the Repeating Unit Conformations I–VIII

	I	II	III	IV	V	VI	VII	VIII
					E′-(1 → 3)-**A**			
ϕ	97	92	91	91	96	91	97	98
ψ	−125	−134	−130	−133	−130	−131	−128	−127
					A-(1 → 4)-**B**			
ϕ	−71	−77	−64	−71	−91	−88	−73	−75
ψ	121	120	126	121	115	116	121	121
					B-(1 → 6)-**C**			
ϕ	−87	−79	−83	−90	−85	−66	−83	−82
ψ	−176	173	−101[a]	172	−165	−172	170	−170/−105[b]
ω	−167	62	−156	57	−163	175	59	−158
					C-(1 → 6)-**D**			
ϕ	91	94	88	92	100	82	97	99
ψ	178/−140[b]	159	−174	174	−171	175	177	−175
ω	−162	−162	−173	−167	−74	60	−83/−163[b]	−76
					D-(1 → 6)-**E**			
ϕ	88	88	98	99	103	95	97	91
ψ	−161	−159	173	−171	−174	−160	−162	−179
ω	−171	−171	60	60	−160	−161	−162	55
					E-(1 → 3)-**A″**			
ϕ	99	98	95	89	95	90	101	88
ψ	−121	−125	−126	−136	−126	−135	−122	−140
					A″-(1 → 4)-**B″**			
ϕ	−81	−89	−94	−89	−90	−80	−79	−90
ψ	111	106	104	106	104	110	109	106
					F-(1 → 3)-**B**			
ϕ	−84	−76	−91	−76	−80	−77	−76	−77
ψ	−105	−100	−107	−104	−97	−95	−101	−98

[a] Deviating average value due to transition, see text.
[b] Average value of distinct regions in MD simulation.

the superposition of several frames from the MD trajectory of II (Figure 5). Furthermore, hydrogen bonds between non-neighboring residues are frequently observed. The most predominant hydrogen bond, observed in all MD runs, exists between the hydroxyl groups **F** OH-3 and **A** OH-6. The presence of this hydrogen bond in all simulated repeating unit conformations confirms the relative rigidity of the **A** → [**F** →]**B** fragment. Five-membered ring forms adopt envelope or twist conformations that differ little in energy.[18] Inspection of the five-membered ring of residue **F** show that during all MD simulations a large number of transitions between different puckering conformations occurred. Due to the position of **F** in the side chain, the shape of its ring has little influence on the global shape of the molecule. No clear correlation between the ring conformations and the presence of the hydrogen bond between **F** OH-3 and **A** OH-6 is observed. The MD trajectories show no transitions of the glycosidic dihedral angles for the (1 → 3)- and (1 → 4)-linked residues, and only a few for the (1 → 6)-linked residues. The ψ angle of the **C** → **D** linkage in the MD trajectory of I reveals a transition

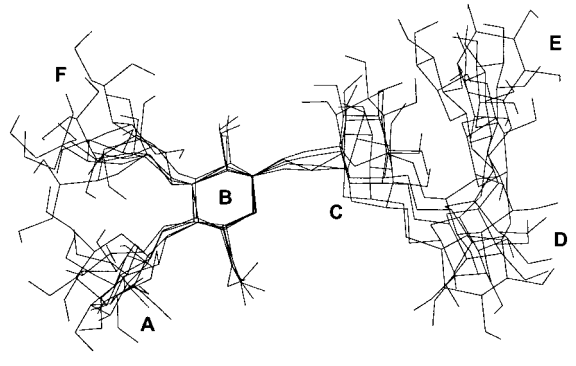

FIGURE 5 Starting conformation of II, along with four conformations within the same conformational space.

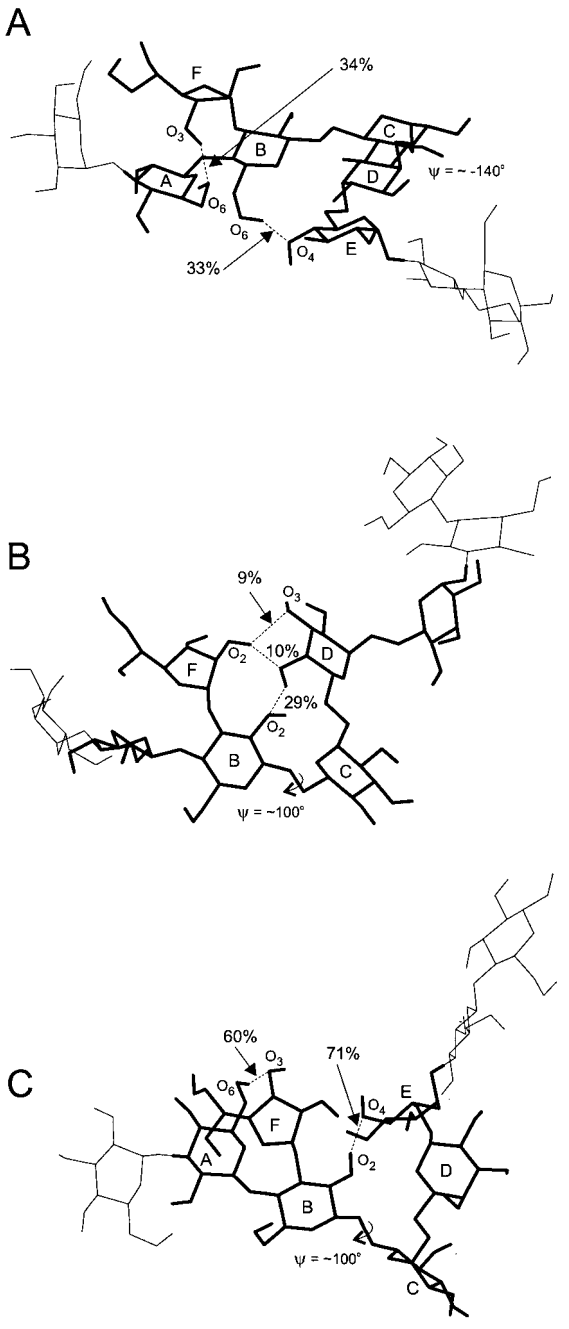

FIGURE 6 Snap shot of the MD trajectory of conformation (A) I, (B) III, and (C) VIII, illustrating hydrogen bond formation between non-neighboring residues.

from 178° to −140°. Inspection of I after the transition suggests that the intramolecular hydrogen bond between **B** OH-6 and **E** OH-4 (Figure 6A) is of importance in stabilizing conformation I with $\psi = -140°$. The ψ angle of the **B** → **C** linkage in conformation III reveals an instantaneous transition of this dihedral from its starting value of 178° (Table I) to the low probability average value of −101°. Observed intramolecular hydrogen bonds between hydroxyl groups of residues **B** and **D**, and **F** and **D** (Figure 6B) are likely to stabilize this conformation. For the **B** → **C** linkage a similar transition is observed in the MD trajectory of VIII ($\psi = -170°$ to $\psi = -105°$). Here the intramolecular hydrogen bond between **B** OH-2 and **E** OH-4 is probably the stabilizing factor of the conformation in which $\psi = -105°$ (Figure 6C). In the MD simulation of VII a transition of the ω angle in the **C** → **D** linkage from approximately −83° to −163° after about 0.2 ns, converts VII into the more stable conformation II.

Polysaccharide Building

From the conformational ensembles generated by the MD simulations of I–VIII, polymer structures can be constructed by connecting randomly selected conformations from these ensembles. If polymers are constructed from conformations of different ensembles, their selection is in random order, but in accordance with the relative occurrence of the ensembles. Oligosaccharide structures of typically 10 repeating units are generated possessing single repeating unit conformers I–IV (Figure 7A). Oligosaccharides solely composed of repeating unit conformers V–VIII are not evaluated, since the occurrence of multiple repeating units with these conformations are, due to their low molar ratios (Table III), not likely. The generated models differ with respect to their secondary structure. The oligosaccharides built from I and III have extended structures with nonuniform bents. The oligosaccharide model built from II shows a helix-like structure, in which multiple repeating units form one helical turn. The structure of IV is less regular than II, but still possesses a helix-like turn. From conformers I to VIII a polysaccharide model containing 100 repeating units is generated using the molar ratios obtained from the AUS simulations (Table III). This degree of polymerization is less than 10% of the average size of EPSs produced by lactic acid bacteria.[19] The obtained polysaccharide model (Figure 7B) gives a plausible description of the conformations of the polysaccharide chain in solution. It exhibits a flexible twisted secondary structure and tends to adopt a random coil conformation as a tertiary structure.

CONCLUSIONS

For the EPS produced by *L. helveticus* 766 it was found that the global and local energy minima ob-

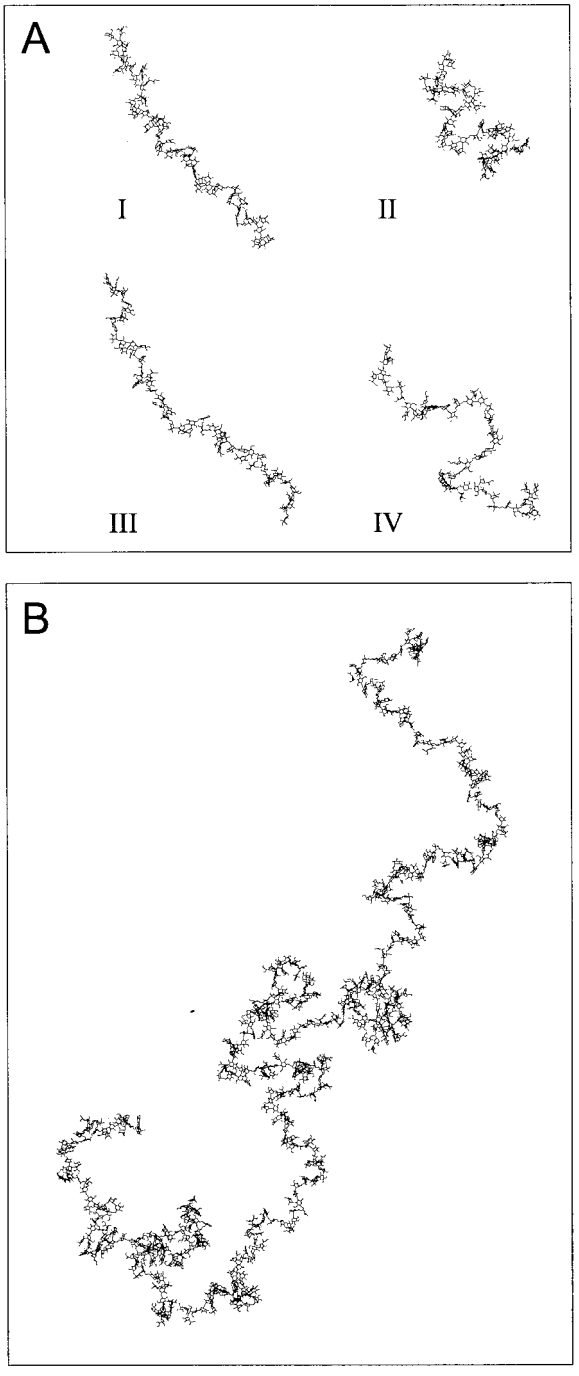

FIGURE 7 (A) Oligosaccharide structures generated from I to IV and (B) polysaccharide structure generated from I to VIII in a molar ratio according to Table III. The oligosaccharide chains consist of 50 and the polysaccharide chain of 500 backbone residues (10 and 100 repeating units).

tained by MM calculations for the constituting disaccharide fragments are good starting points to explore the conformations of this polysaccharide. Adaptive umbrella sampling of the potential of mean force was applied successfully to obtain rotamer distributions of flexible glycosidic dihedral angles in solution. The MD simulations of the most probable conformations of the elongated repeating unit **2** indicate only minor differences in the trajectory-averaged dihedral angles in comparison with the same dihedral angles obtained from the AUS simulations. The few transitions, which do occur, are probably caused by the interaction of some non-neighboring residues. For the prediction of the conformation of polysaccharides it is important to study oligosaccharide fragments of a certain size in order to include the most prominent long-range interactions. This may lead to an iterative process since these long-range interactions may only become apparent during the building of a polysaccharide from previously obtained repeating unit conformations. It must be kept in mind that the interactions of nonbonded residues can influence the ratio of different local conformations in the polysaccharide, because this ratio was based on AUS simulations of smaller oligosaccharide fragments. This holds especially for the EPS produced by *L. helveticus* 766, since the presence of three consecutive (1 → 6)-linkages within the repeating unit make the EPS very flexible, and therefore a large number of different long-range interactions are possible. Including these effects in the AUS simulations by extending the oligosaccharide fragments for these simulations is not feasible, since all conformational differences in the free dihedral angles have to be taken into account during the AUS simulations. The construction of oligo- and polysaccharide models demonstrates the secondary and tertiary structure of the *L. helveticus* 766 EPS. Characterization of these polysaccharide models in terms of persistence length will be subject of further research.

This study was supported by the PBTS Research Program with financial aid from the Ministry of Economic Affairs and by the Integral Structure Plan for the Northern Netherlands from the Dutch Development Company.

REFERENCES

1. MacGregor, E. A.; Greenwood, C. T. Polymers in Nature; John Wiley & Sons: Chichester, 1980; pp 240–328.
2. Cerning, J. FEMS Microbiol Rev 1990, 87, 113–130.
3. Faber, E. J.; Kamerling, J. P.; Vliegenthart, J. F. G. Carbohydr Res 2001, 331, 183–194.
4. Rao, V. S. R.; Qasba, P. K.; Balaji, P. V.; Chandrasekaran, R. Conformation of Carbohydrates; Harwood Academic Publishers: Amsterdam, 1998; pp 223–254.

5. Robijn, G. W.; Imberty, A.; van den Berg, D. J. C.; Ledeboer, A. M.; Kamerling, J. P.; Vliegenthart, J. F. G.; Pérez, S. Carbohydr Res 1996, 288, 57–74.
6. Xu, Q.; Bush, C. A. Biochemistry 1996, 35, 14521–14529.
7. Robijn, G. W.; Thomas, J. R.; Haas, H.; van den Berg, D. J. C.; Kamerling, J. P.; Vliegenthart, J. F. G. Carbohydr Res 1995, 276, 137–154.
8. Grootenhuis, P. D. J.; Haasnoot, C. A. G. Mol Simul 1993, 10, 75–95.
9. Kouwijzer, M. L. C. E.; Grootenhuis, P. D. J. J Phys Chem 1995, 99, 13426–13436.
10. Hooft, R. W. W.; van Eijck, B. P.; Kroon, J. J Chem Phys 1992, 97, 6690–6694.
11. Van Gunsteren, W. F. GROMOS, Groningen Molecular Simulation Package: University of Groningen: The Netherlands; 1987.
12. Spieser, S. A. H.; van Kuik, J. A.; Kroon-Batenburg, L. M. J.; Kroon, J. Carbohydr Res 1999, 322, 264–273.
13. Berendsen, H. J. C.; Postma, J. P. M.; van Gunsteren, W. F.; Hermans, J. In Intermolecular Forces; Reidel: Dordrecht 1981; pp 331–342.
14. Ryckaert, J.-P.; Ciccotti, G.; Berendsen, H. J. C. J Comput Phys 1977, 23, 327–341.
15. IUPAC-IUB Joint Commission on Biochemical Nomenclature Eur J Biochem 1983, 131, 5–7.
16. Kroon-Batenburg, L. M. J.; Kroon, J.; Leeflang, B. R.; Vliegenthart, J. F. G. Carbohydr Res 1993, 245, 21–42.
17. Poppe, L. J Am Chem Soc 1993, 115, 8421–8426.
18. Perez, S.; Kouwijzer M.; Mazeau K.; Engelsen S. B. J Mol Graphics 1996, 14, 307–321.
19. Sikkema, J.; Oba, T. Snow Br R&D Reports 1998, 107, 1–31.